Article

Computational Fluid Dynamic Study with Comfort Analysis in Large Atrium of the Angelo Hospital in Venice

Margherita Ferrucci [1,*], Piercarlo Romagnoni [1], Fabio Peron [1] and Mauro Strada [2]

1 Laboratorio di Fisica Tecnica Ambientale, Università Iuav di Venezia, 30135 Venezia, Italy; pierca@iuav.it (P.R.); fperon@iuav.it (F.P.)
2 STEAM S.r.l. Architettura e Ingegneria, 35131 Padova, Italy; mstrada@steam.it
* Correspondence: marferit@gmail.com

Abstract: To improve the thermal comfort in the hall of the Angelo Hospital (Venezia) an analysis was developed by using Computation Fluid Dynamics and considering some configurations for the air-conditioning system and for the solar shading devices. The reference configuration consists of the installation of four fan coils in the area coupled with a 3 m high metal casing used for solar shading. Then, three other solutions are proposed: by increasing the number of fan coils and changing their position, by adding some radiant panels arranged on the walls, and by inserting a physical confinement as a lateral confinement. The study consists of three sections. Firstly, a section in which the study area is modelled through a strong simplification that allows to represent only a slice of the domain but to immediately evaluate the role of the casing. A second section in which the area is completely modelled, and a third section in which a comfort evaluation is carried out. The analysis shows that the metal casing brings a substantial benefit due to the solar shielding it causes. The radiant panels cool the area only near the wall. The increasing of the number of the fans leads to an excessively high air speed and localized discomfort due to drafts. The lateral confinement on the north and south side is the one that guarantees better cooling of the study area.

Keywords: computation fluid dynamics simulations; Large Eddy Simulation; thermal comfort; Predictive Mean Vote (PMV); Predicted Percentage of Dissatisfied (PPD); Draught Rating (DR)

1. Introduction

In recent decades, extensive atria and halls have been inserted with increasing frequency by architects in public building like sport arenas, train stations, airport halls, luxury hotels, hospitals, museums, and multistory office buildings [1–5]. The main aims were to increase penetration of natural illumination and to create exchange areas where to manage the flow of people and where visitors can socialize. A non-conditioned atrium can serve as a thermal buffer decreasing building energy consumption for winter heating. If it is continuously occupied specific kind of air conditioning is necessary to maintain thermal comfort and energy consumption increases [6]. Various researchers analysed the indoor environmental conditions and the design of halls and atria in relation to energy performance, natural light, and comfort [7]. This is not a simple task.

From the point of view of lighting performance in many studies was defined as geometry is very important. Shape, size height, ratio of glazing to opaque surfaces are the parameters that are of great significance to optimize the atrium environment (e.g., [8–11]). Geometric parameters are also important with regard to fire safety and energy consumption for air conditioning. Lan studied the impacts of atria's geometric configuration on indoor thermal condition and energy consumption in different climate conditions in China [12]. Aldawoud analysed the impact of the atrium shape on the total energy consumption and identified the most energy-efficient atrium design [13]. Ayala considered the effect of roof geometry on fire development obtaining good agreement between experiments and numerical simulations [14].

From the point of view of thermal environment, complicated thermal and fluid dynamics phenomena could take place in these confined spaces. Experimental analysis with multipoint measurements of environmental conditions and computational fluid dynamic are the two investigation strategies that can be adopted. Kato et al. [15] developed a Computational Fluid Dynamics analysis of an atrium characterized by a height of 130 m sandwiched between two high-rise office buildings. They obtained the flow and temperature fields and demonstrated how in summer natural ventilation can limit the excessive increase in the air temperature in the upper part. A comparison study between simulation and measurements of thermal parameters of a fully conditioned atrium in Ottawa was presented by Laouadi [16]. The predicted temperatures were within 2–3 °C of measured temperatures. Gan et al. analysed the thermal performance of an atrium integrated with photovoltaic (PV) modules [17]. By mean of CFD was investigated the effect of ventilation strategies on PV modules temperature and as consequence on their performance. Abdullah conducted a field study on the application of internal solar blinds and water spray, to minimize air overheating in an atrium in tropical climate [18]. Liu et al. presented an effective methodology for evaluating the ventilation performance of an atrium building in the design stage, applying CFD and reduced-scale models (P. Liu, 2009). In simulation RNG k—ε and zero-equation turbulent schemes demonstrated to be very efficient. The correct positioning of stack openings can create a direct ventilation path and improve the quality of the indoor thermal environment. Tanasic et al. studied the airflow in industrial halls using as a case study a paper mill [19]. The accuracy of the simulation was evaluated by comparing its results with data coming from field measurements. Simulations demonstrated to be a useful tool for qualitative analysis. Hussain verified the application of various turbulence models (standard k-ε, RNG k-ε, 'realizable' k-ε, and SST k-ε) in CFD simulation of an atria building with a hybrid ventilation system. The comparison with quite extensive measurements indicates that CFD model agree well with the measurements with all turbulence model but SST k-ε give results closer to measured data [20].

Lu et al. analysed performances of atria during winter in severe cold climate, establishing a zonal model, and measuring in a case study infiltration air flows [21]. When comparing the simulated and measured data they obtained, a good agreement with a maximum air temperature deviation of 1.2 °C was found. Albuquerque et al. investigated the use of the internal thermal mass and natural ventilation to control the conditions inside an atrium in a non-residential building. Numerical simulation and experimental data were in good agreement, and it has been seen that with this strategy the cooling load has decreased around 30% [22]. Wu et al. [23] utilized CFD simulation supported by on-site measurements to parametrically study the influence of geometry on the energy and lighting performance of an atrium during the summer in China. They analysed the atrium thermal environment comprehensively from the aspects of air temperature, surface temperature, and vertical temperature difference. In certain climatic areas, atria can be characterized by environmental conditions with a low level of comfort and moreover cooling and heating energy consumption can be extremely huge due to the cold winter and/or penetration of sun radiation in hot summer. A possible strategy to improve comfort conditions and limit energy consumption can be to identify the areas more frequented by people and to locally air-conditioning these areas [24,25]. Knowledge of the design conditions (type of environment, user comfort and air quality) must be combined with specific knowledge of the characteristics of the system terminals, their positioning and the thermal effects induced in the environment. The use of scale models and/or numerical calculation methods is however desirable, but absolutely must not be taken as the only reference [26].

Following this path, the analysis of the entrance hall of the Ospedale dell'Angelo in Venice is proposed in this paper as a case study. The tool used is that of computational fluid dynamics supported by a limited number of experimental surveys. Some localized climate control strategies were analysed in waiting areas for outpatients awaiting specialist visits based on the use of fan coils and radiant panels and on the confinement of the space to be air-conditioned. A check of direct solar radiation was likewise analysing. Using the

comfort model proposed by Fanger [27], the level of well-being for visitors was assessed in correspondence with the various system solutions, identifying a specific design proposal capable of guaranteeing a level of comfort corresponding to the client's objectives.

2. The Case Study

The Angelo hospital ("Ospedale dell'Angelo") is located in Mestre, a western district of Venezia (Italy) at these geographic coordinates 45.51 N, 12.22 E in a large commercial area. The hospital is divided into several buildings surrounded by a vast green area (117,600 m^2 out of a total of 260,000 m^2). The green area is mainly sown with grass and also has some trees with a purely decorative function, and which do not function as solar shielding. The building, designed by Studio Altieri with the advice of the Argentine architect Emilio Ambasz, was delivered in 2008 [28]. The building is characterized on one side by inclined glass window exposed from east to south-west and on the other by hanging terraces. The entire structure is 31 m high, with the glass facade of 24 m high (see Figure 1 for the top view, Figure 2 for the frontal elevation and the Figure 3 for the south-west and north-east side view). The inclined glazed canopy consists of a steel, glass and aluminium structure and is 7000 m^2 large, 180 m long at the base and 160 m at the top. The canopy is made up of 1100 pieces of glass, each different from the other because the façade is convergent and therefore each piece has a particular curvature. The glass facade borders the hall that welcomes visitors and in which there are also some shops and a garden. The hall, originally intended as a central hub and sorting to the hospital wards, later became a waiting point for patients.

On the platform located on the 1st floor it is located the outpatient area (coloured in red, Figure 4). This zone, totally immersed in the large volume of the atrium, is exposed to solar radiation. The prismatic hall is conditioned only in some areas, such as on the ground floor and partially in the outpatient area (the study area) where there is a noticeable thermal discomfort for staff and patients, especially during the summer season. Effectively the glass façade exposed to solar radiation is not provided with solar screens, and since each glass element is different from the others, as well as the considerable size of the facade, it makes the installation of a solar radiation protection or modification of the canopy very complex. The installation of the latter would bring many advantages, but it has been excluded by the administration for the complexity and cost. Some waiting areas of the platform were already affected by interventions to improve comfort. These interventions consisted of having created completely confined and air-conditioned spaces in the platform (like as air conditioning box). These actions, although efficient from a thermal point of view, have not had the desired effects. In fact, people waiting, prefer to stay outside the air-conditioned area than inside, because this is not in front of the clinics.

During this previous intervention, some experimental temperature measurements had been carried out at various points in the platform [29]. The measurements were recorded both during the winter and the summer period. We extrapolated the data of the average temperature of the air in the summer during the month of July. The measurements were made during the hottest hours of the day: at 10 and 11 A.M., at 14 and 15 P.M. The outdoor temperature at 10 A.M. was 24 °C and the maximum outdoor temperature was 34.50 °C at 14 P.M. Under these two external conditions, the temperatures on the platform were 24 °C at 10 A.M., and, starting from 11 A.M., temperatures growth over 28 °C. The maximum recorded temperature was 28.9 °C at 12 A.M. Therefore, these measurements were taken as a reference to analyse the case study, to propose technical solutions and then to assign the boundary conditions to our models.

Under these circumstances other solutions have been proposed, studied, and presented here. The suggested technical configuration consists of the addition of a 3 m high metal casing with a slightly rounded shape used for solar shading and lateral confinement of the area coupled with four fan coils that cools the zone. Then other solutions are proposed: by increasing the number of the fan coils and changing their distribution in space, by adding

some radiant panels arranged on the walls (see Figure 5) and by inserting two lateral physical confinements (like doors or air-jet), [30].

A partial and non-exhaustive study of the technical proposals and their effects on the thermal comfort was developed in [31]. In this paper, all the study phases are deeply developed, and the relevant computational fluid dynamics results are reported in addition to the thermal comfort analysis.

The study has been carried out by using computational simulations for analysing the indoor conditions after the installation of the technical devices. CFD techniques allow to study large, confined spaces, where it is difficult to predict the indoor air flows and thermo-hygrometric fields by means of simplified models or measurements [32]. The fluid dynamics analysis allows on the one hand to have a spatial representation of the air velocity fields and its temperature and to immediately understand the influence of a technical device such as the metal casing or a fan coil. On the other hand, it allows us to extrapolate useful data for the computing of the PMV and PPD comfort indices in the outpatient area. The work is split into three sections:

- The first section introduces the CFD model, the characteristics of the numerical grid (see Section 3.1) and the thermal comfort models (Section 3.2).
- In the second section (Section 4) the preliminary phase of the study is developed by using CFD simulations with strong simplifications on a slice of the model.
- In the third section (Section 5), four configurations (the reference configuration and the A, B and C configurations) are analysed by CFD simulations. With the latter is possible to evaluate the general and local thermal comfort for each design solution.
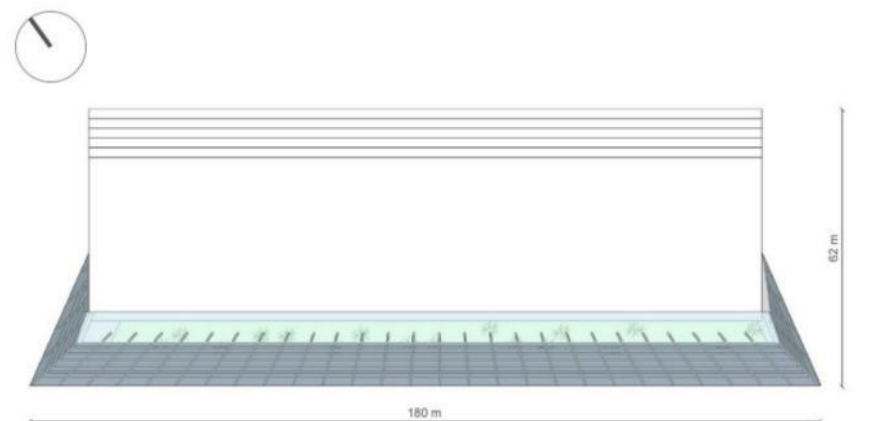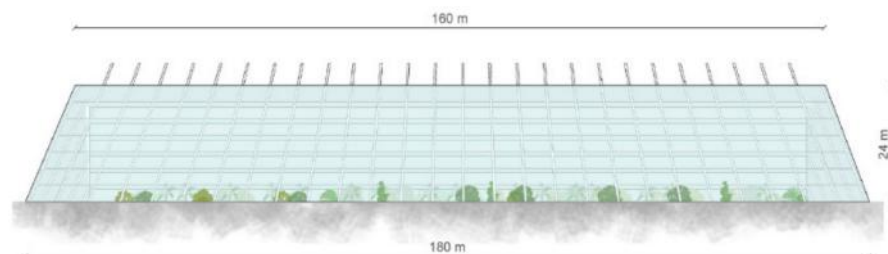

Figure 1. Top view of the building [33].

Figure 2. Frontal elevation (south-east side) [33].

Figure 3. South-west and north-east side view [33].

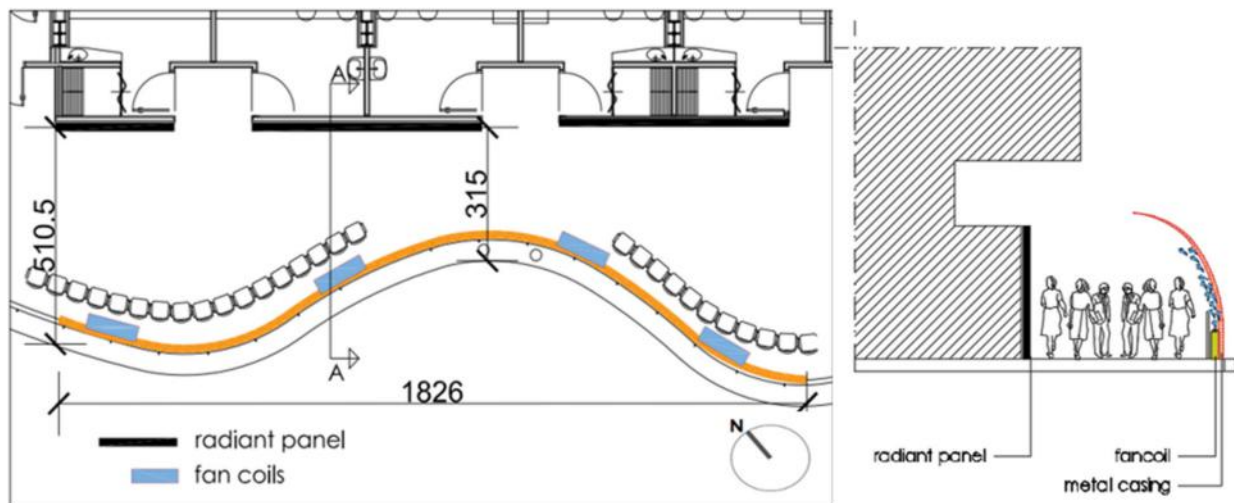**Figure 4.** Section south-east north-west of the building (in red the outpatient area).

Figure 5. Plan of the intervention area on the left, section AA, on the right, showing the outpatient area and the technical solutions (fan coils, radiant panels, metal casing) proposed and analysed. The units of the quotas are in centimetres.

3. The Numerical Models and the Comfort Indices

3.1. The Computational Fluid Dynamics Model

The code used for the CFD simulations is Fire Dynamics Simulator (FDS) coupled with the graphical interface Pyrosim. The FDS numerically solves a form of the Navier-Stokes equations appropriate for low-speed (Ma < 0.3) thermally-driven flow by using the very-large eddy for turbulent model. Since FDS was designed to simulate thermally-driven flows within buildings the simplest and most efficient mesh (numerical grid) is the rectilinear, structured and uniform one. FDS approximates the governing equations on a rectilinear

mesh. Rectangular obstructions are forced to conform with the underlying mesh. Once the dimensions of the grid are established, it is necessary to define the rectangular obstructions that fill the grid, to define the geometry of the model at the level of resolution determined by the size of the grid. This method is the Immersed Boundary Method that was first proposed by Peskin [34] who developed it to simulate blood flow through the mitral valve of the heart. In general, this method simplifies the meshing process reducing computation times for simulations [35]. Thermal boundary conditions are assigned for all solid surfaces. The equations of the flow motion are approximated using the finite difference method with second-order accuracy on uniformly spaced three-dimensional grids. Hence, the needs to have the most regular and structured mesh possible [36,37].

The calculation time steps are variable with the Courant Friedrichs Lewy (CFL) number sets between 0.8 and 1.

The adopted mathematical model for turbulence is the Very Large Eddy Simulation. This model differs from the Large Eddy Simulation in that it calculates the CFL number considering the norm of the velocity vector equal to the maximum intensity of a component of a velocity calculated in the cell (hence the "very large"). This choice allows reducing the computation time compared to the LES.

The LES approach is based on the following observations: the larger turbulent structures, in addition to having anisotropic characteristics and dependent on the specific problem, constitute the most significant energy contribution ("energy-containing eddies") and therefore are responsible for most of the effects: increased transport/mixing; increase in friction and heat exchange coefficients; conversely, the smallest (dissipative) structures are essentially isotropic and universal, that is, they do not depend on the specific problem (geometry).

The equations for large-eddy simulation are derived by applying a low-pass filter, known as a Favre filter, to the transport equations for mass, momentum, and energy (that are the same of Direct Numerical Simulation equations). In FDS, the filter width is equivalent to the local cell size and is a key parameter in the submodels for the turbulent viscosity. The goal of the LES is to evolve the cell mean values of mass, momentum, and energy explicitly, while accounting for the effects that the subgrid transport have on the mean fields. To this end a filter to the DNS equations is applied to obtain the filtered equations [38].

Therefore, with LES, through a non-stationary 3D simulation, the spatial and temporal scales of greater dimension (Large Eddies) are directly captured, asking an appropriate model, the SubGrid Scale model, the task of taking into account the effects of the smaller scales not resolved [39,40]. In LES, the "turbulence model" refers to the closure for SGS flux terms. In FDS, gradient diffusion is the turbulence model used to close both the SGS momentum and scalar flux terms. We then require a model for the turbulent transport coefficient: the turbulent (or eddy) viscosity or the turbulent (or eddy) diffusivity. The turbulent diffusivity is obtained using a constant Schmidt number (for mass diffusivity) or Prandtl number (for thermal diffusivity), and so the most important transport coefficient is the turbulent viscosity set 0.1 by the Deardoff model.

3.2. The Thermal Comfort Evaluation

The general thermal comfort is evaluated in some strategic points of the area, by calculating the comfort Predicted Mean Vote index according to [41,42] and the discomfort index with Predicted Percentage of Dissatisfied. Then the local thermal discomfort by the Draught Rate index, that expresses the percentage of dissatisfied with the presence of a draft, is computed. There are four points where comfort was assessed: three points are in the middle of the corridor (between the casing and the clinics) distributed along the entire length of the waiting area. Finally, the fourth point was chosen in the middle of the length of the corridor at a distance of 0.6 m from the metal casing. This choice simulates the position of waiting (seated or standing relaxed) people who can be found or in the centre of the corridor or seated near the casing (in this area there are currently chairs).

Concerning the PMV calculation, the metabolic rate is fixed for a standing relaxed/seated person with light clothing and environmental conditions are obtained by CFD simulations. In particular, the mean radiant temperature (Tmrt), the air temperature (T_{air}), the air humidity (h) and the air velocity (v) are necessary. The Mean Radiant Temperature and the Effective Radiant Field are computed by using SolarCal tool [43] that predicts the impact of solar radiation on occupant thermal comfort by computing the solar heat absorbed and liberated in clothing and skin. The parameters chosen for each configurations in SolarCal tool take in account the environment in summer season so: the solar altitude h = 69°, the solar horizontal angle relative (α_{hr}) to front of person (α_{hr} = 110°), the direct beam (normal) solar radiation equal to 225 W/m², the total solar transmittance of the glass facade τ = 0.44, the sky vault view fraction 1.41, the fraction of body exposed to sun 0.5, the average shortwave absorptivity α_{sw} = 0.67.

The PPD index, obtained from the PMV index, provides information on thermal discomfort by predicting the percentage of people likely to feel too hot or too cold in the given thermal environment. The thermal dissatisfaction may be caused by an unwanted cooling of one specific part of the body. We also compute the index draught rating DR, according to [44].

4. Preliminary Phase: CFD Simulation of a Slice of the Model

In this preliminary phase three simulations were performed representing a "slice" of the model: one configuration with the metal casing (PA), one without the metal casing (PB) and one simulation with the metal casing but with a modification on the boundary conditions (PA_1). This preliminary phase allows us to choose more reliable boundary conditions that will be adopted for the next model too, and above all allows us to quickly understand the influence of metal casing and fan-coils. In fact, the representation of a slice of the model greatly reduces the computational cost of the simulations. The model represents a portion of the analysed area and the space that goes from the clinics (in yellow) to the glass façade (in blue). The dimensions of the domain are 25.5 m long, 6.8 m high and 0.5 m large (see Figure 6).
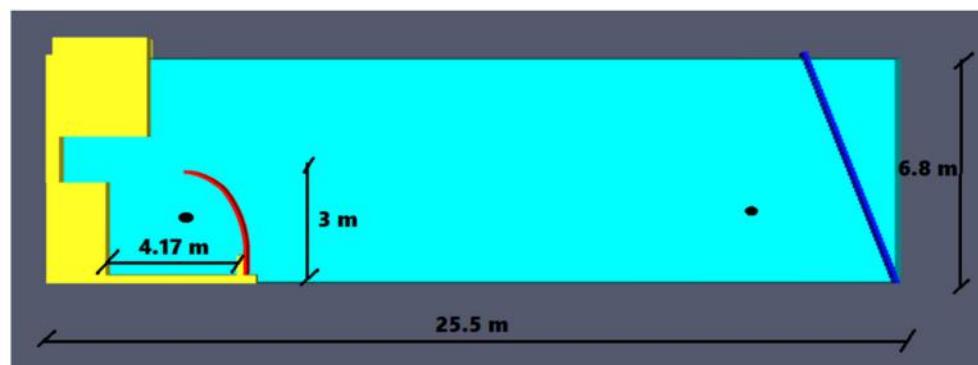

Figure 6. The slice model: dimensions and control point (in black).

A mesh sensitivity study is performed to identify the most suitable size for the calculation. The control points are located in the centre of the corridor and beyond the metal casing (see Figure 6).

- The domain is split into 18,481 cubic elements.
- The characteristics of the grid are:
- Number of cells: 18,481 (154 in *x* direction, 3 in *y* direction, 40 in *z* direction),
- Dimensions of the cells: 0.1669 m (*x*-axis), 0.1667 m (*y*-axis), 0.1703 m (*z*-axis).
- Size ratio of the cells: 1 (*x*-axis), 1 (*y*-axis), 1.02 (*z*-axis).
- The simulation becomes stationary after 250 s of computing.

The fan coil is positioned next to the carter; the volume flow (q) is set q = 0.09785 m^3/s. The temperature of the air-jet is T_{air} = 15 °C. These values are calibrated by following the technical data sheet of a real fan coil of 132 cm long with q = 930 m^3/h.

The effect of sun radiation was taken into account setting a heat flux on surfaces equivalent to the power adsorbed and exchanged by convection with internal environment. On the metal carter is applied a heat flux (h_f) equal to h_f = 0.3 kW/m^2 with emissivity ε = 0.55. On the glass façade is applied an h_f = 0.2 kW/m^2. The temperature of wall of the clinics and the temperature of the soil (in yellow) are set T_{wall} = 27 °C. The air temperature to initialize the computation is set T_{air} = 28 °C. On the lateral borders:

- On the right (next to the glass facade) there is an open boundary with T_{air} = 34.5 °C. This is a maximum summer temperature recorded in the site during the previous experimental campaign.
- On the left, a solid border is set, with a surface temperature of T_{wall} = 27 °C and emissivity ε = 0.9.
- On the top the boundary, the condition is an open condition with the temperature T_{air} = 28 °C and the relative pressure Pr = −1.0 Pa. The slightly negative pressure simulates the suction activated by the "solar chimney effect" of the top of the glass façade. This value is assigned in agreement with the measurements carried out by the previous experimental campaign.
- On the bottom the boundary condition there is an open condition with the air temperature T_{air} = 28 °C and the relative pressure Pr = +0.1 Pa. This value is assigned in agreement with the measurements carried out by the previous experimental campaign.

On the front and on the back the "mirror" condition is set for the configurations PA and PB, For the PA_1 configuration we set an "open" boundary condition. We recall that the mirror condition denotes a symmetry plane with no flow across de boundary. The open condition denotes a passive opening to the outside.

CFD Results of the Preliminary Phase

The Figure 7a–c show the air temperature distribution for the PA configuration (a), for the PB configuration in the absence of a metal casing (b) and when the open boundary condition is set (c), (PA_1 configuration).

The metal casing prevents the flow from falling into the atrium. The mirror condition imposes a repetition of the condition indefinitely. Therefore, on the one hand, the capacity of the fan coil is overestimated and on the other, the confinement provided by the metal casing is enhanced. The visual results of the simulation indicates that the design idea can work but the slice modelling remains a partial study and a more detailed numerical model is need. The study shows how the presence of the metal casing next to the fans is essential to direct the flow of cold air in the outpatient gallery and not to disperse the flow in the atrium.

(a)
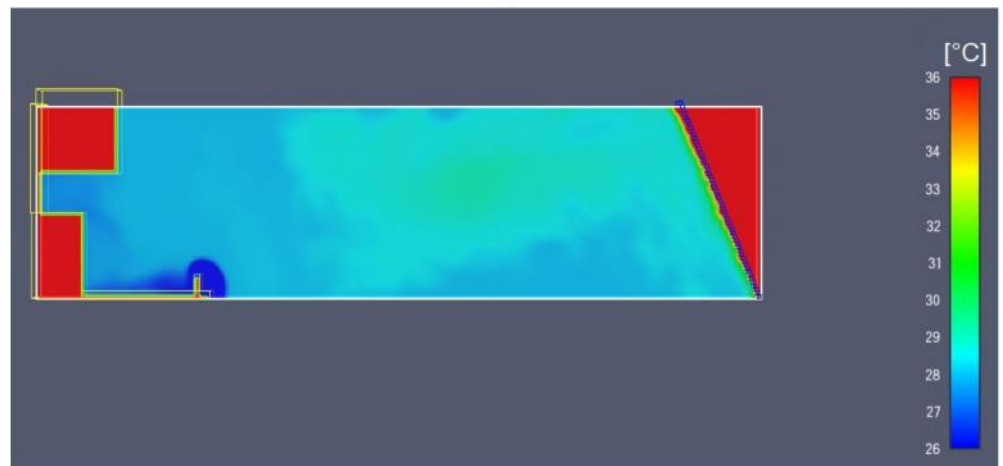
(b)
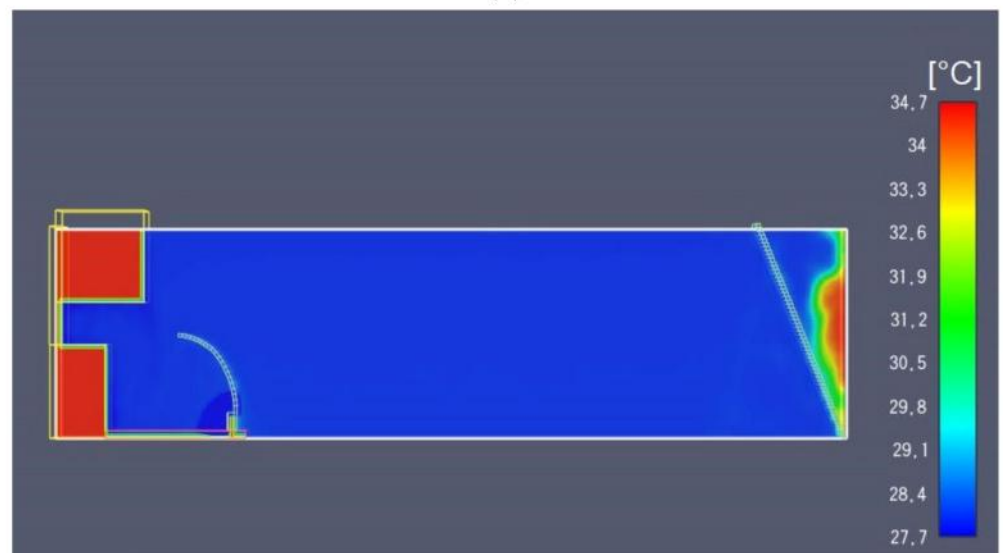
(c)

Figure 7. Air temperature distribution [°C] at time step t = 250 s for: PA configuration (**a**), PB configuration without carter (**b**) and PA_1 (**c**).

5. Detailed Analysis Phase of the Complete Model

5.1. CFD Simulations

The geometry of the outpatient platform is 3D-modelled, including the 3 m high metal casing and the fan coils. The domain is 20 m long, 7 m height and 11 m width. The configurations modelled are the following:

- The reference configuration: the metal casing that boards the outpatient area + 4 fans following the plans in Figure 5, (see Figure 8).
- A configuration: (metal casing + 5 fans, equal to the reference configuration plus 1 fan), see Figure 8.
- B configuration: equal to the reference configuration with the addition of radiant panels installed on the walls at a surface temperature of $T_{rad} = 17\,^{\circ}C$, see Figure 9.

C configuration: equal to the reference configuration with the addition of a physical confinement (like doors or air-jet) on the south side and the north side of the study area (metal casing + 4 fans + radiant panels), see Figure 9.
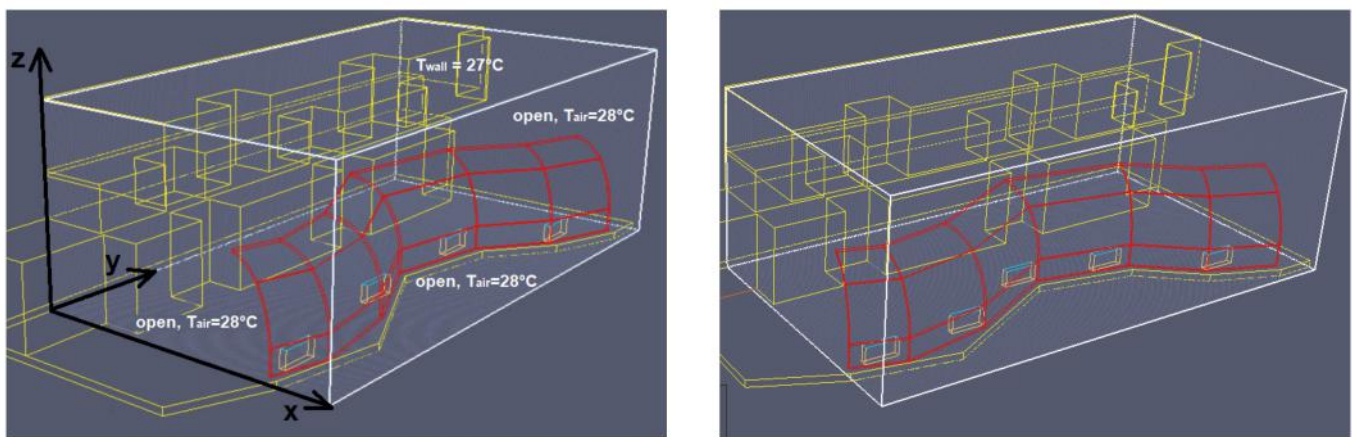

Figure 8. (**On the left**): reference configuration (4 fan coils and metallic carter) with boundary conditions. (**On the right**): the A configuration with the 5 fan coils.
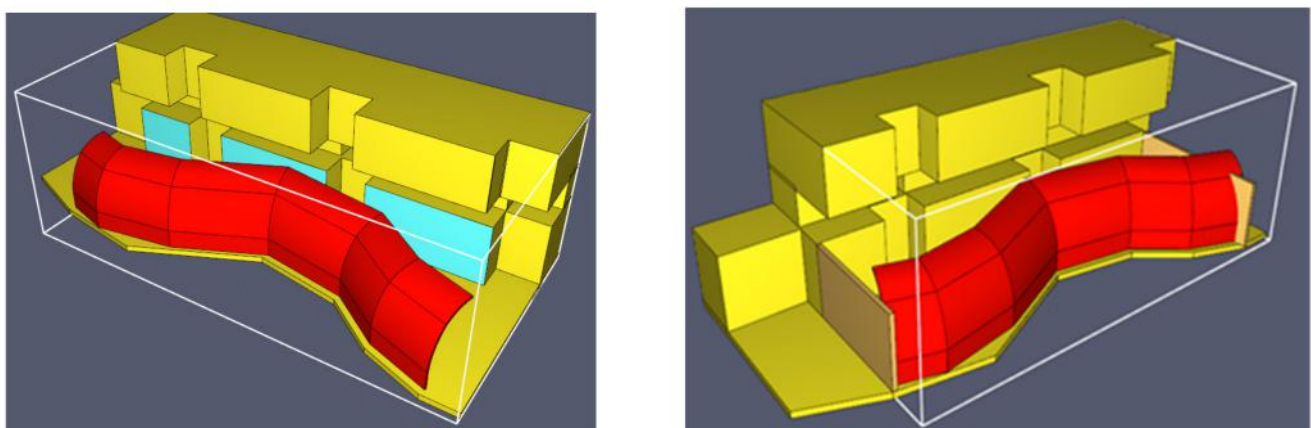

Figure 9. (**On the left**): B configuration with radiant panels arranged on the wall adjacent to the clinics. The panels are marked in blue. (**On the right**): C configuration, geometric model with south and north side confinement.

As consequence the number of the fan coils changes in function of the configuration: four fan coils in the reference configuration (following the plans in Figure 5), five fan coils in A configuration and again four fan coils in B and C configuration. The fan coils are

fully modelled, following the technical data sheet (dimensions $220 \times 590 \times 1320$ mm and $q = 930$ m^3/h).

The domain is split into 1,454,112 cubic elements (length side: 0.1 m) and the characteristics of the uniform grid are:

- Number of cells: 1,454,112 (108 in x direction, 198 in y direction, 68 in z direction),
- Dimensions of the cells: 0.0995 m (x-axis), 0.0997 m (y-axis), 0.0993 m (z-axis).
- Size ratio of the cells: 1 (x-axis), 1 (y-axis), 1 (z-axis).

The analysis on the sensitivity of the proposed mesh was performed before to choose the dimension of the cells. They were 3 different meshes: Normal ($82 \times 150 \times 52$ number of cells), Fine (that presented before and chosen with $108 \times 198 \times 68$ number of cells) and Finer ($134 \times 35 \times 84$ number of cells). We compared the temperatures and the velocities obtained with the three different meshes. For the temperatures we compared the temperatures of the points T1, T2, T3 and T4 (see Table 1) during the calculation time. We observed that with a "large grid" (called the normal size) the temperatures were even 2 °C h higher than the fine and finer mesh, and often these last were superposed. Then, we observed that after 400 s of computation a steady state was reached. We also compared the velocities resulting (after 400 s of calculation) for the three different mesh sizes. We superposed the results of all points (the total line) at the centre of the corridor with a height to the platform above 1.56 m. In this case, the results of the normal and fine mesh are quite harmonious (see Figure 10).

Table 1. Coordinates of the control points.

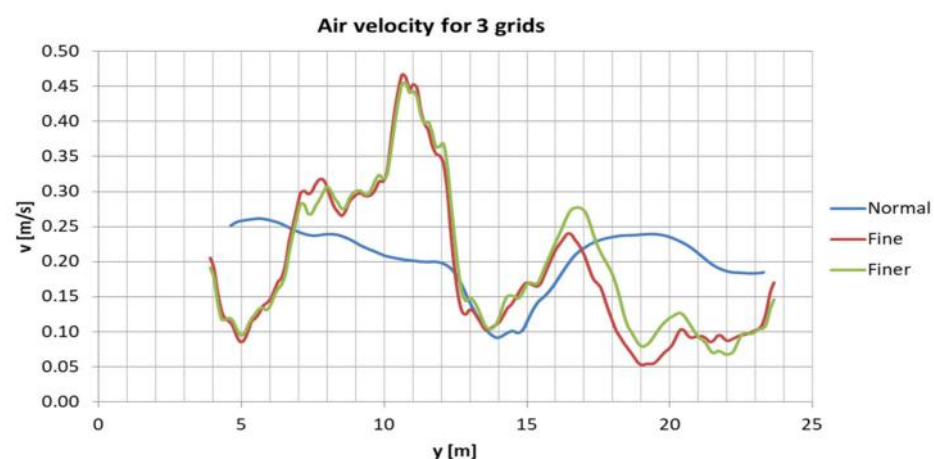|	Control Points	X: Distance to the Wall [m]	Z: Height above the Platform [m]
	T1	0.85	0.561
Inside the carter	T2	0.85	1.561
	T3	2.67	0.661
Outside the carter	T4	5.93	0.661

Figure 10. Sensitivity study. The results of the control points in the centre of the corridor with $x = 1.5$ m, $z = 1.56$ m are for three different meshes: the normal, the fine and the finer. In the x-axis the air velocity in [m/s], in the y-axis the coordinate [m] along the corridor (see Figure 8 for the reference).

The following boundary conditions are assigned:

- At the floor and over the walls the surfaces temperature is $T_{wall} = 27$ °C and emissivity $\varepsilon = 0.9$.
- The temperature of the air at the exterior of the domain is set $T_{air} = 28$ °C.
- The pressure is set equal to the atmospheric pressure.
- On the carter we assigned a net heat flux $h_f = 0.3$ kW/m^2 with emissivity $\varepsilon = 0.55$.

- For each fain coil the airflow temperature is set T_{air} = 15 °C, and the airflow q = 930 m³/h (the rest of the machine is inert).
- For B configuration the radiant panels have a surface temperature of T_{rad} = 17 °C (emissivity ε = 0.9).
- For C configuration the physical confinement (like doors or air-jet) on the south side and the north side of the study area is set as inert.
- In all lateral borders, except the ambulatory side border, the condition of "open boundary" with an air temperature T_{air} = 28 °C.
- On the solid border corresponding with the ambulatory boundary is set a surface temperature T_{wall} = 27 °C and emissivity ε = 0.9.

All simulations were stopped upon reaching the steady state condition (400 s). The check was performed by comparing the values of the 36 temperature and air velocity control points that were placed in the domain. We dispose a series of four points (T1, T2, T3, T4) at the positions y equal to 5 m, 8 m, 10 m, 14 m, 16 m, 18 m, 20 m, 21.5 m and 23 m. The coordinates x and z of the points are described in the Table 1 and the position in the Figure 11. The slices to visualize the air velocity distribution and the air temperature distribution are positioned as shown in Figure 11.
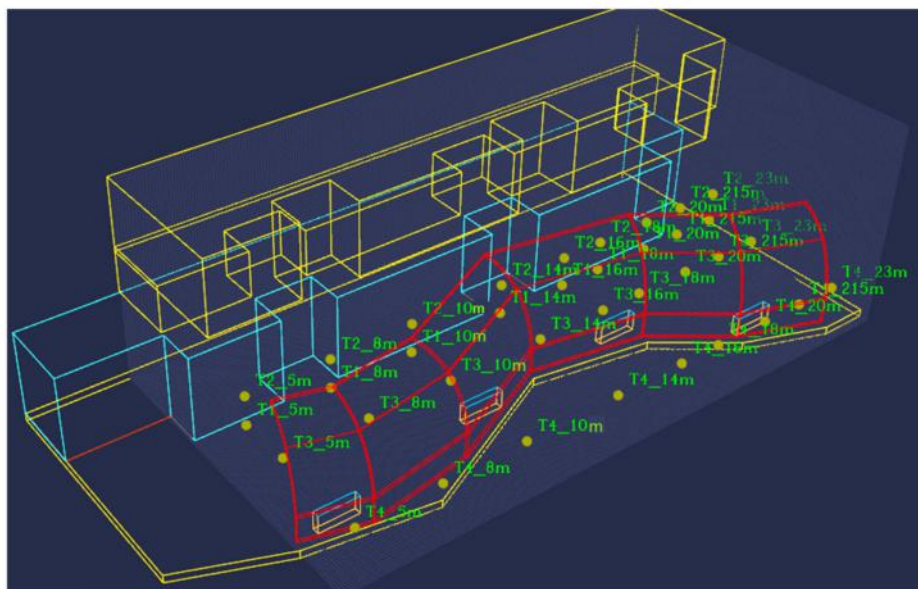

Figure 11. Visualization of the control points.

The air temperature distributions in Figures 12–14 and in the velocity field in Figure 15 are shown for the reference configuration. In Figure 16, the temperature distribution of the three configurations is compared for the horizontal section z = 1.1 m on the platform.

In Figure 17, the air velocity distribution for A, B, and C configuration is shown. The air temperature probes T1, T2, and T3 are compared below for each configuration (Figure 18). This nomenclature is used to identify the configuration and position of the probe: Ti_Y_Config, with i = 1,2,3 and Y = 5 m, 10 m, 14 m, 18 m. The configuration shown is that for y = 10 m and the probe T3 y = 18 m. In Figure 19, we compare the air temperature for the four configurations (REF, A, B, and C). We compare the points at the same height (z = 1.1 m) at three different positions: y = 5 m; 10 m, and 16 m.
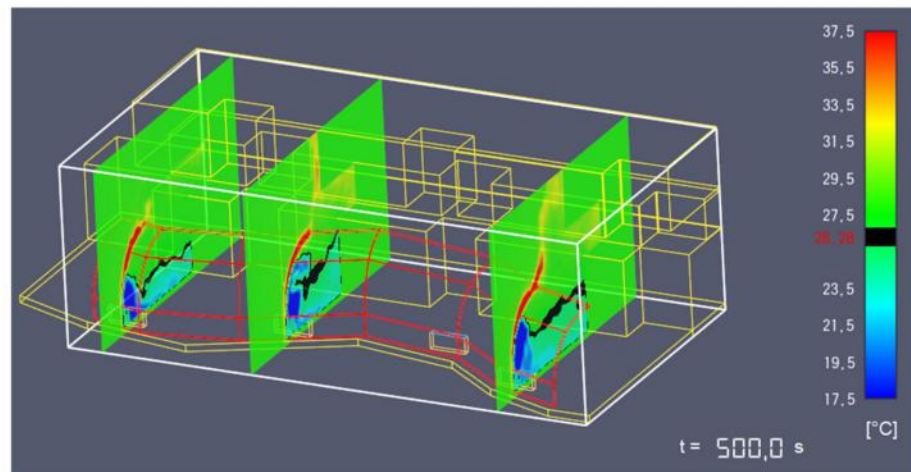
Figure 12. Reference configuration: air temperature distribution in the section y = 5 m, 10 m, 20 m, t = 500 s.
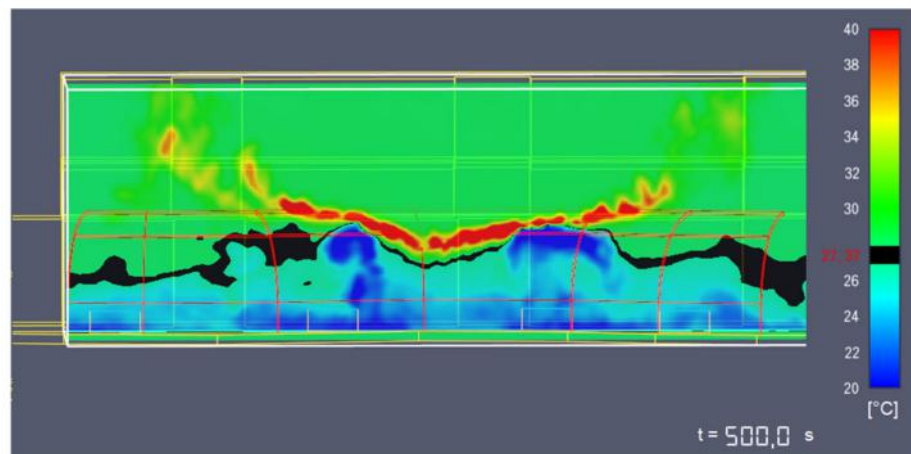

Figure 13. Reference configuration: air temperature distribution in the section x = 3.1 away from the wall, t = 500 s.
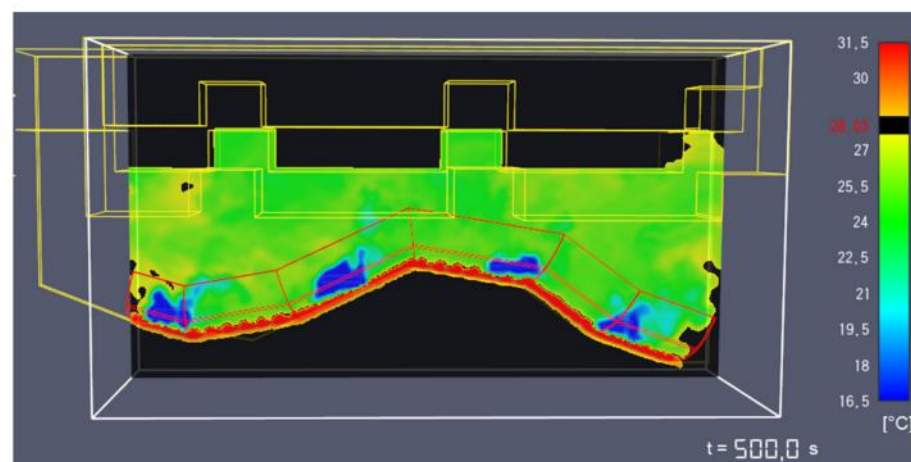

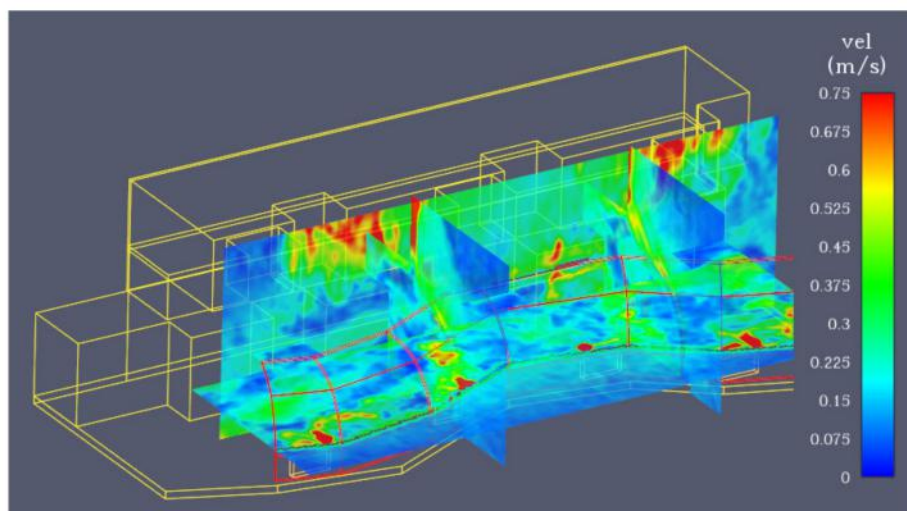**Figure 14.** Reference configuration: air temperature distribution in the horizontal section z = 1.1 m at t = 500 s.

Figure 15. The reference configuration: velocity fields [m/s] at t = 500 s.

5.2. Comfort Analysis

The comfort is evaluated in four points: three localized in the centre of the corridor at a height above the floor of 1.1 m (for y = 5, 10, 18 m), modelling the thermal sensation of a standing relaxed person (or seating person not relaxed person) (1.2 met) (see Figure 20).

One point at z = 0.6 m, y = 14 m at 0.6 m far from the carter, modelling the thermal sensation of a seated person (1.0 met). The clothing level is set 0.6 clo, the relative humidity at 50%. The results are summarized in Table 2.

Table 2. PMV, PPD and DR of the configuration in 4 points.

| Config.	z = 1.1 m, y = 5 m, x = in the Middle of the Corridor					z = 1.1 m, y = 10 m, x = in the Middle of the Corridor					z = 1.1 m, y = 18 m, x = in the Middle of the Corridor					z = 0.6 m, y = 14 m, x = Next to the Metal Casing				
MRT	28.5 °C					28.5 °C					28.5 °C					30 °C				
	T_{air} °C	v m/s	PMV	PPD %	DR %	T_{air} °C	v m/s	PMV	PPD %	DR %	T_{air} °C	v m/s	PMV	PPD %	DR %	T_{air} °C	v m/s	PMV	PPD %	DR %
REF	23.55	0.12	0.62	13	11	25.5	0.17	0.21	6	15	25.1	0.3	0.32	7	23	25	0.2	0.32	7	12
A	23	0.27	0.17	6	21	24	0.26	−0.05	5	20	22.1	0.3	−0.29	7	28	23.6	0.15	0.18	6	9
B	23	0.11	0.24	6	13	23.55	0.2	−0.10	5	17	22.1	0.3	−0.05	5	28	22.3	0.17	0.14	5	11
MRT for C	26 °C					26 °C					26 °C					29 °C				
C	25.1	0.17	0.04	5	5	21.5	0.12	−0.28	7	9	22.4	0.12	−0.46	9	16	24.5	0.17	0.17	6	12
	T_{air} °C	v m/s	PMV	PPD %	DR %	T_{air} °C	v m/s	PMV	PPD %	DR %	T_{air} °C	v m/s	PMV	PPD %	DR %	T_{air} °C	v m/s	PMV	PPD %	T_{air} °C

For a seated person the Effective Radiant Field is 34.8 W/m^2 with a Mean Radiant Temperature variation DT_{mrt} = 8.3 °C. Considering that the ambient air temperature T_{air} = 28.5 °C and the air velocity v = 0.1 m/s we compute for the current configuration (without the carter and fan coils) the PMV = 2.51 and PPD = 94%.
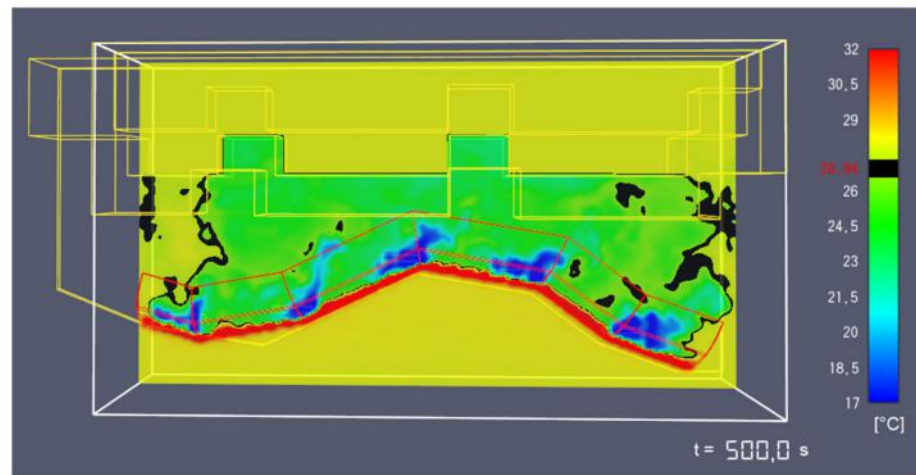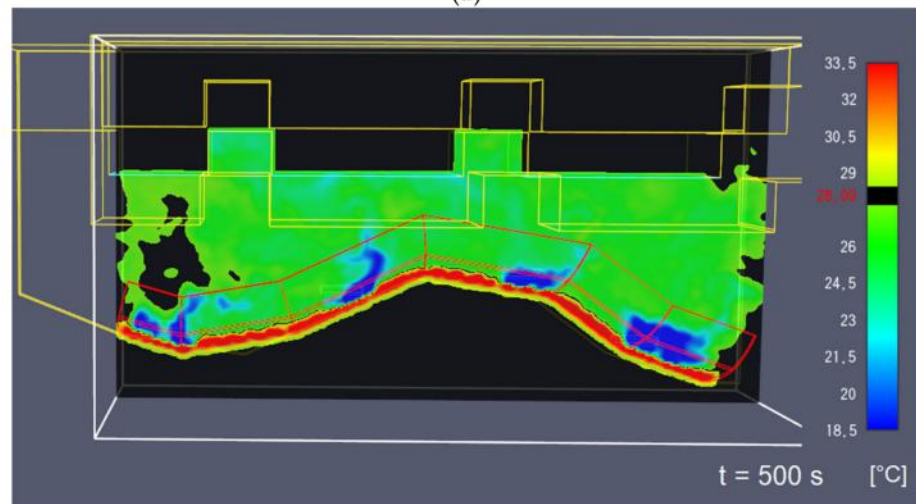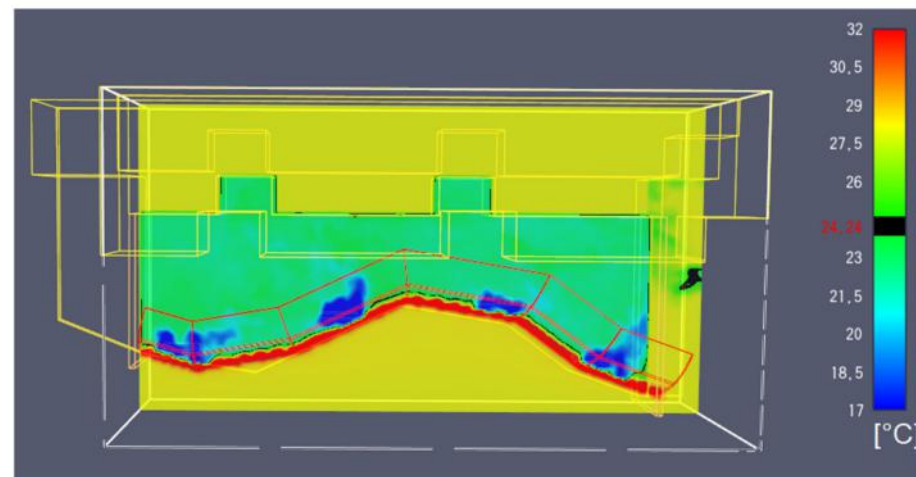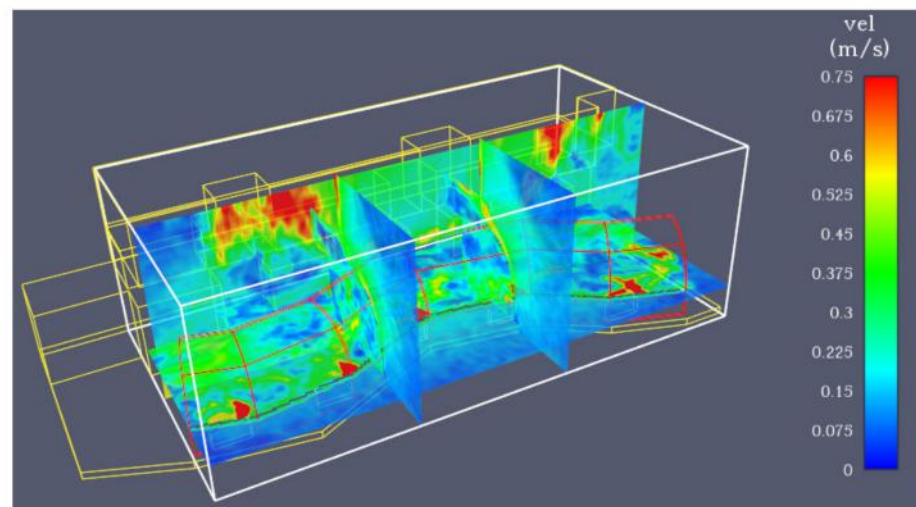
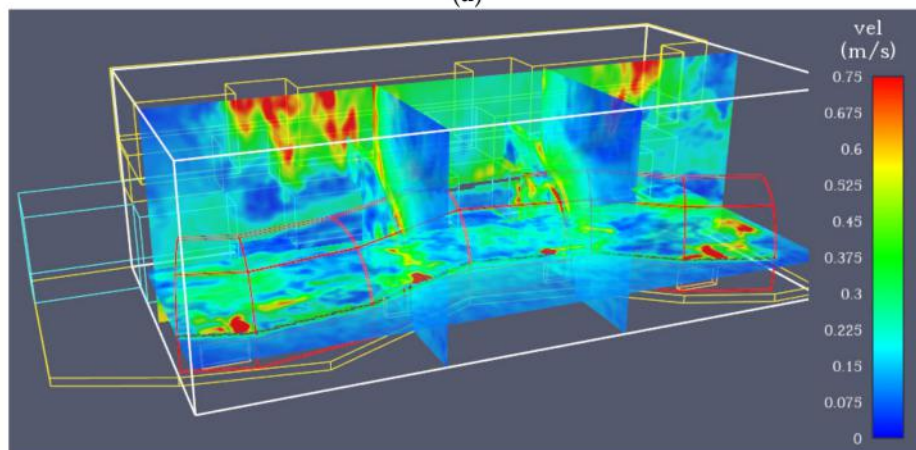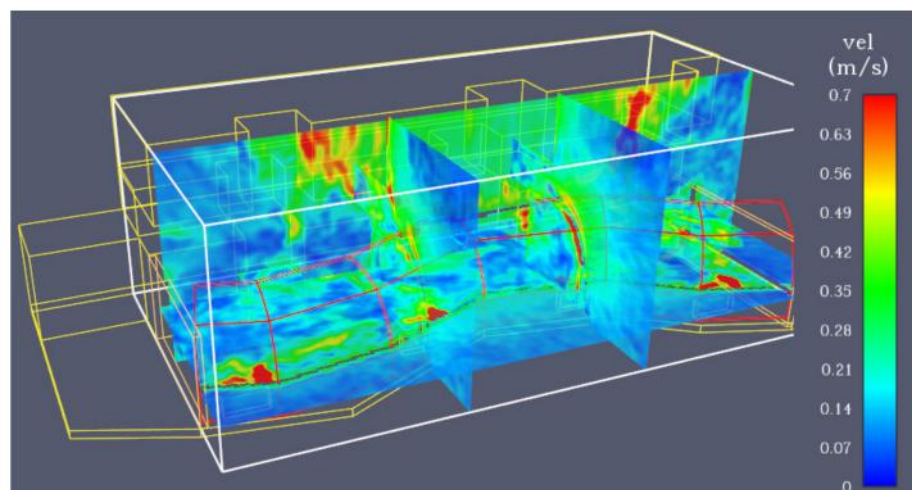**Figure 16.** Air temperature distribution in the horizontal section z = 1.1 m, t = 500 s: (**a**) A configuration; (**b**) B configuration; and (**c**) C configuration.

Figure 17. Air velocity fields at t = 500 s for: (**a**) A configuration; (**b**) B configuration; and (**c**) C configuration.
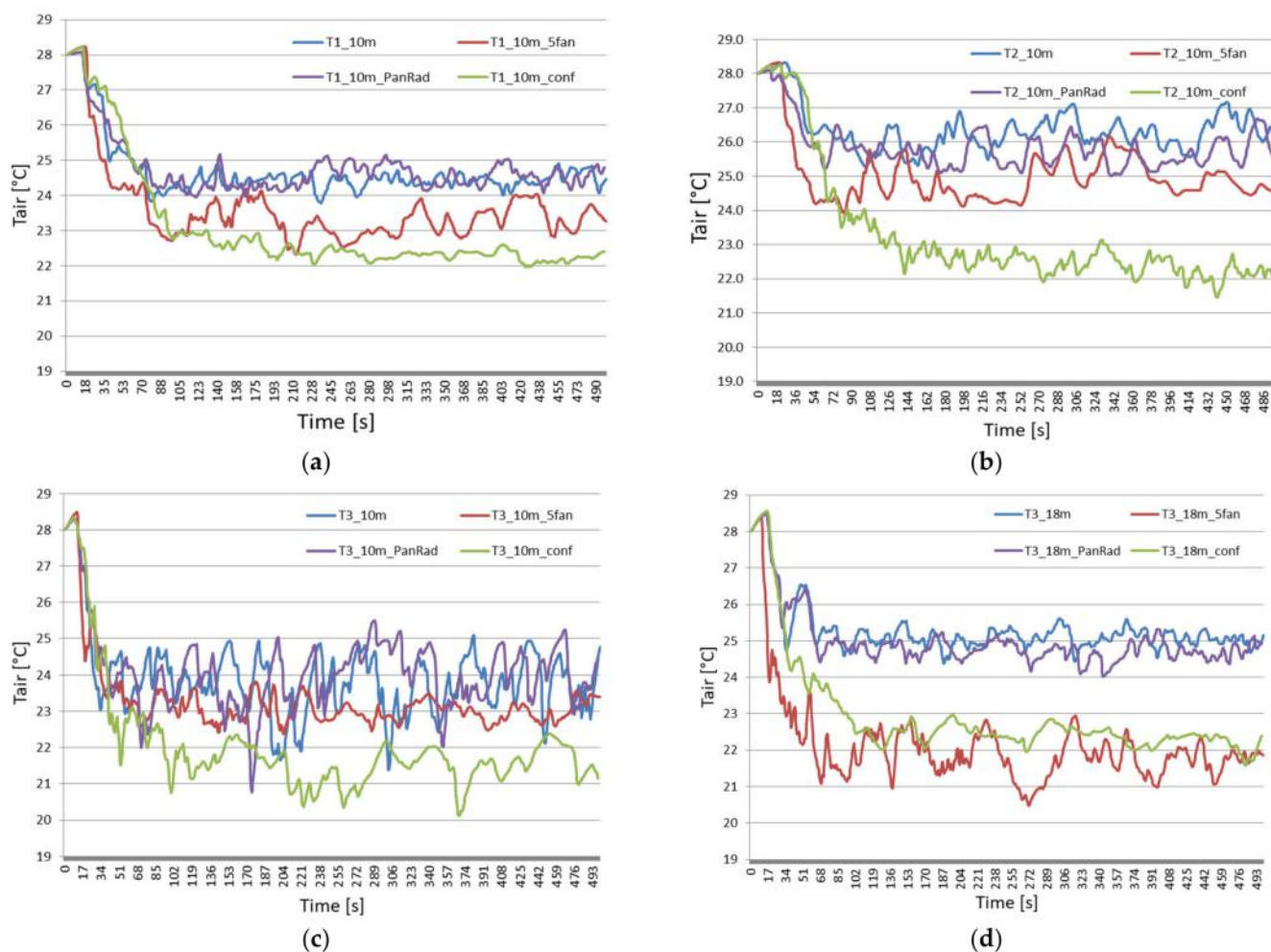
Figure 18. Simulated air temperatures trends for the control points T1_10 m (**a**), T2_10 m (**b**), T3_10 m (**c**), T3_18 m, (**d**) (see the Table 1 for the coordinates).

The Mean Radiant Temperature changes in function of the position of the points and configurations. In particular MRT is $T_{mrt} = 28.5\ °C$ in the centre of the area, it grows until $T_{mrt} = 30\ °C$ next to the carter for the reference configuration, for the A and C configuration. For the B configuration (with radiant panel) the $T_{mrt} = 26\ °C$ in the centre of the area and grows until $T_{mrt} = 29\ °C$ next to the metallic casing.

5.3. Results

From the first simulations it is observed that the effect of the casing is beneficial and prevents the flow from falling into the atrium. For this to be optimized, the casing must be located as close as possible to the fan coils in order to prevent the flow of fresh air from remaining behind the machines.

From an analysis that takes into account only the value of the temperatures extrapolated from the CFD simulation, it is observed that C (with confinement on the north and south side) is the configuration that guarantees better cooling of the study area. The results of this configuration suggest that if adopted, the air flow rates of the fans could be reduced to cut down the energy demand. The solution with five fan coils greatly improves cooling compared to the solution with four fan coils. The radiant panels cool the area only near the wall and are much less effective than the two other solutions.

The comfort study shows that the metal casing brings a substantial benefit due to the solar shielding. The reference configuration seems to be satisfactory, while that with five fan coils could induce a feeling of risk of DR higher than the other solutions.
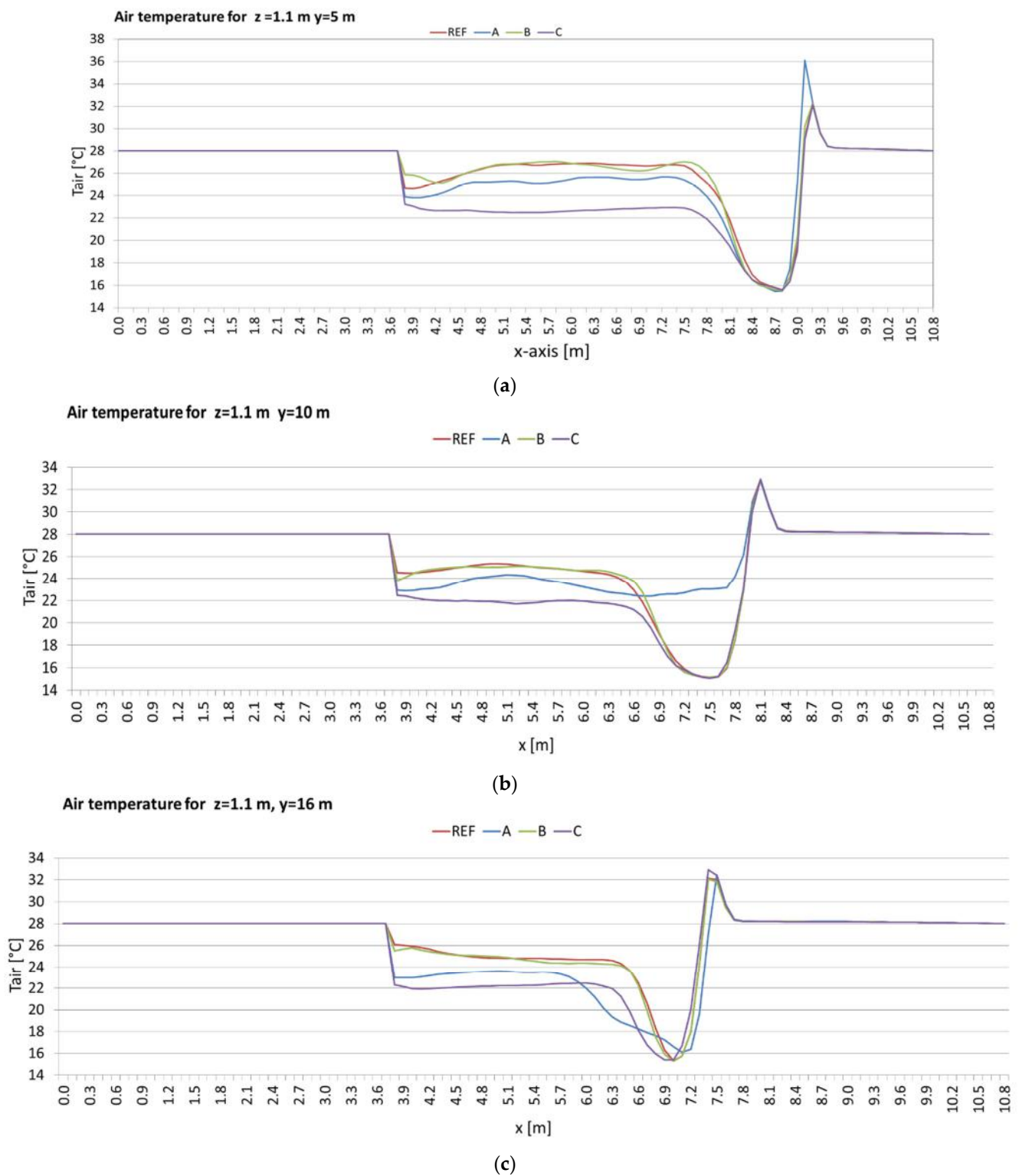
(**a**)

(**b**)

(**c**)

Figure 19. Comparison between the air temperatures for the four configurations (REF, A, B, and C). We compare the points at the same height ($z = 1.1$ m) at three different positions: $y = 5$ m; 10 m, and 16 m) shown in graphic (**a**–**c**). The width of the corridor is represented on the x axis (see the reference system in the Figure 10).
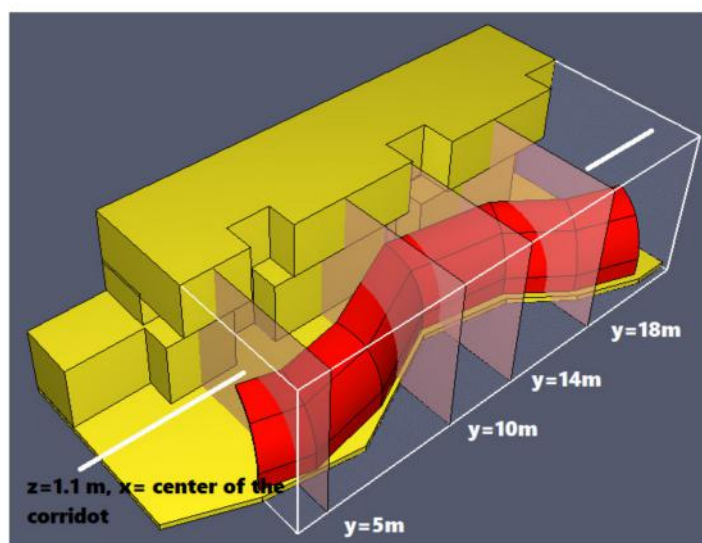
Figure 20. Geometrical model.

The effect of lateral confinement and insertion of the radiant panels slightly increases the sensation of cold. These two options could give more neutral values if we increase the clo value slightly (we consider 0.6 clo, that is very low). The punctual values of the PMV, PPD and DR calculated for such a large area, even if they have been chosen so that they are representative points of the most frequent positions for patients, are not sufficient to indicate the distribution of comfort in the whole zone. For this reason, it is important to use and to associate the images of the results (air velocity and air temperature distributions) of the CFD simulations to the values the comfort indexes. As further development, the study should therefore be deepened with a calculation of punctual comfort and discomfort in all calculation nodes of the grid as shown in a previous study developed with the same team [45].

6. Conclusions

Research activity has consisted of a detailed analysis of the total air flow paths, velocity fields and temperature distribution in the outpatient area of the hall in a hospital during the summertime. Indoor air flows and the thermal fields were simulated by using CFD and the resulting environmental conditions were compared. The code used for the CFD simulations was Fire Dynamics Simulator coupled with the graphical interface Pyrosim. FDS solves numerically a form of the Navier-Stokes equations, appropriate for low-speed thermally-driven flow by using the very-large eddy for turbulent model. Two types of simulations were effectuated: one on a «simple model, consisting in a slice of a full model (preliminary phase), and one on a complete model of the outpatient area. The preliminary phase of the study, representing the slice of the model, allowed us to choose more reliable boundary conditions that have been adopted for the next model too. Then, it allowed us to quickly understand the influence of metal casing and fan-coils. In fact, the representation of a slice of the model greatly reduces the computational cost of the simulations. Despite the significant simplification of the model, it was possible to extrapolate useful indications and effectuate a qualitative analysis of the area. Four configurations were analysed by CFD simulations with a model fully representing the outpatient area. With the latter was possible to evaluate the general and local thermal comfort for each design solution.

- The effect of the metal casing is beneficial, and it prevents the flow from falling into the atrium. Thus, the presence of the metal casing next to the fans is essential to direct the flow of cold air in the outpatient gallery and not to disperse the flow in the atrium;
- On one hand, the thermal comfort indices allowed a first and easy assessment of the effectiveness of the proposed system, on the other the indices calculated only at

some point in the outpatient waiting area do not take into account the large size of the study area;

- The differences in the distribution of flows can be observed in the distribution of air temperatures and air velocity in the CFD results images. This means that it becomes important to analyse the effect of the technical devices, not only by looking at the comfort and discomfort indices but also by considering the maps of the distributions of air velocity and temperatures.

Local environmental control strategy combining shading and air cooling was applied in a part of a large atrium and discussed. In the state-of-the-art review, very few studies on similar conditions were found. Although the data of an experimental campaign were used to calibrate the boundary conditions of our model, we do not have experimental data to confirm the goodness of the simulation results. This is a research limitation which will be overcome once construction on the site has begun. Given the problems linked to the COVID-19 pandemic, it has not been possible to conduct the intervention in the hospital. When construction is completed, an experimental campaign will be performed on site, and the research can be deepened.

Conflicts of Interest: The authors declare no conflict of interest.

References

1. De Santoli, L.; Caruso, G.; Mariotti, M. Ventilation Design in Large Enclosures for Sports Events using CFD: The Halls of the "Città dello Sport" in Rome. In Proceedings of the Clima 2007 WellBeing Indoors, Helsinki, Finland, 10–14 June 2007.
2. Meng, Q.L.; Li, Q.; Zhao, H.; Li, L.; Chen, Z.L.; Chen, Y. Numerical study on airflow and temperature distribution in an airport terminal building under natural ventilation. In Proceedings of the IAQVEC 2007, sixth International Conference on Indoor Air Quality, Ventilation and Energy Conservation in Buildings: Sustainable Built Environment, Sendai, Japan, 28–31 October 2007.
3. Vujošević, M.; Krstic-Furundzic, A. The influence of atrium on energy performance of hotel building. *Energy Build.* **2017**, *156*, 140–150. [CrossRef]
4. Stamou, A.I.; Katsiris, I.; Schaelin, A. Evaluation of thermal comfort in Galatsi Arena of the Olympics "Athens 2004" using a CFD method. *Appl. Therm. Eng.* **2008**, *28*, 1206–1215. [CrossRef]
5. Zhao, B.; Li, Y.; Li, X.T.; Yan, Q.S. Numerical analysis and improvement of air flow pattern for the Great Hall of the People. *Build. Therm. Energy Vent. Air Cond.* **2000**, *4*, 5–8.
6. Danielski, I.; Nair, G.; Joelsson, A.; Froling, M. Heated atrium in multy-storey apartment buildings, a design with potential to enhance energy efficiency and to facilitate social interactions. *Build. Environ.* **2016**, *106*, 352–364. [CrossRef]
7. Moosavi, L.; Mahyuddin, N.; Ghafar, N. Atrium cooling performance in a low energy office building in the Tropics, a field stuy. *Build. Environ.* **2015**, *94*, 384–394. [CrossRef]
8. Calcagni, B.; Paroncini, M. Daylight factor prediction in atria building designs. *Sol. Energy* **2004**, *76*, 669–682. [CrossRef]
9. Ghasemi, M.; Noroozi, M.; Kazemzadeh, M.; Roshan, M. The influence of well geometry on the daylight performance of atrium adjoining spaces: A parametric study. *J. Build. Eng.* **2015**, *3*, 39–47. [CrossRef]
10. Mohsenin, M.; Hu, J. Assessing daylight performance in atrium buildings by using Climate Based Daylight Modeling. *Sol. Energy* **2015**, *119*, 553–560. [CrossRef]
11. Fan, Z.; Zehui, Y.; Liu, Y. Daylight Performance Assessment of Atrium Skylight with Integrated Semi-transparent Photovoltaic for Different Climate Zones in China. *Build. Environ.* **2021**, *190*, 107–129. [CrossRef]
12. Lan, W.; Qionga, H.; Qia, Z.; Honga, X.; Yuen, R.K.K. Role of atrium geometry in building energy consumption: The case of a fully air-conditioned enclosed atrium in cold climates in China. *Energy Build.* **2017**, *151*, 228–241. [CrossRef]
13. Aldawoud, A. The influence of the atrium geometry on the building energy performance. *Energy Build.* **2012**, *57*, 1–5. [CrossRef]

14. Ayala, P.; Cantizano, A.; Gutiérrez-Montes, C.; Rein, G. Influence of atrium roof geometries on the numerical predictions of fire tests under natural ventilation condition. *Energy Build.* **2013**, *65*, 382–390. [CrossRef]
15. Kato, S.; Murakami, S.; Shoya, S.; Hanyu, F.; Zeng, J. CFD analysis of flow and temperature fields in atrium with ceiling height of 130 m. *ASHRAE Trans.* **1995**, *101*, 1497.
16. Laouadi, A.; Atif, M.R. Comparison between computed and field measured thermal parameters in an atrium building. *Build. Environ.* **1998**, *34*, 129–138. [CrossRef]
17. Gan, G.; Riffat, S.B. CFD modelling of air flow and thermal performance of an atrium integrated with photovoltaics. *Build. Environ.* **2004**, *39*, 735–748. [CrossRef]
18. Abdullah, A.H.; Meng, Q.; Zhao, L.; Wang, F. Field study on indoor thermal environment in an atrium in tropical climates. *Build. Environ.* **2009**, *44*, 431–436. [CrossRef]
19. Tanasic, N.; Jankesa, G.; Skistadb, H. Cfd analysis and airflow measurements to approach large industrial halls energy efficiency: A case study of a cardboard mill hall. *Energy Build.* **2011**, *43*, 1200–1206. [CrossRef]
20. Hussain, S.; Oosthuizen, P.H. Validation of numerical modeling of conditions in an atrium space with a hybrid ventilation system. *Build. Environ.* **2012**, *52*, 152–161. [CrossRef]
21. Lu, Y.; Xiang, Y.; Chen, G.; Liu, J.; Wang, Y. On-site measurement and zonal simulation on winter indoor environment and air infiltration in an atrium in a severe cold region. *Energy Build.* **2020**, *223*, 110–160. [CrossRef]
22. Albuquerque, D.P.; Mateus, N.; Avantaggiato, M.; da Graça, G.C. Full-scale measurement and validated simulation of cooling load reduction due to night-time natural ventilation of a large atrium. *Energy Build.* **2020**, *224*, 110–233. [CrossRef]
23. Wu, P.; Zhou, J.; Li, N. Influences of atrium geometry on the lighting and thermal environments in summer: CFD simulation based on-site measurements for validation. *Build. Environ.* **2021**, *197*, 107853. [CrossRef]
24. Calay, R.K.; Borresen, B.A.; Holdo, A.E. Selective ventilation in large enclosures. *Energy Build.* **2000**, *32*, 281–289. [CrossRef]
25. Luo, X.; Huang, X.; Feng, Z.; Li, J.; Gu, Z. Influence of air inlet/outlet arrangement of displacement ventilation on local environment control for unearthed relics within site museum. *Energy Build.* **2021**, *246*, 111–116. [CrossRef]
26. Romagnoni, P.; Strada, M.; Traverso, R. La ventilazione negli edifici di grande altezza. In Proceedings of the AiCARR 57th National Congress, Pisa, Italy, 15–18 September 2002; pp. 67–90.
27. Fanger, P. Calculations of thermal comfort: Introduction of a basic comfort equation. *ASHRAE Trans.* **1967**, *73*, 269–274.
28. Mariagrazia, R. *Il nuovo ospedale di Mestre*; Marsilio: Venezia, Italy, 2007.
29. TIFS Ingegneria. *Technical Report: Analisi del Comportamento Termico e delle Condizioni di Comfort Nell'area di Attesa Ambulatoriale Nell'atrio del Nuovo Ospedale di Mestre*; TIFS Ingegneria: Padova, Italy, 2009.
30. Ferrucci, M.; Peron, F. *Technical report: Analisi Fluido Dinamica Dell'area di Attesa Ambulatoriale Dell'ospedale di Mestre*; Università Iuav di Venezia: Venezia, Italy, 2019.
31. Ferrucci, M.; Romagnoni, P.C.; Peron, F.; Strada, M.; Petrola, R. Comfort analysis and improvement in large Atrium: The case study of Angelo Hospital in Venice. In Proceedings of the Roomvent 2020, Torino, Italy, 14–17 June 2020.
32. Heiselberg, P.; Murakami, S.; Roulet, C.A. *IEA—Annex 26 "Energy Efficient Ventilation of Large Enclosures"*; Kolding Trykcente: Kolding, Denmark, 1998; ISSN 1395-7953R9803.
33. Tognon, F. Luce naturale: Alternative Progettuali per il Miglioramento del Comfort Visivo. Master's Thesis, Università Iuav di Venezia, Venezia, Italy, 2018.
34. Peskin, C. Flow patterns around heart valves: A numerical method. *J. Comput. Phys.* **1972**, *10*, 252–271. [CrossRef]
35. Tu, J.; Yeoh, G.H.; Liu, C. *Computational Fluid Dynamics—A Pratical Approach*; Butterworth-Heinemann: Oxford, UK, 2018. [CrossRef]
36. Morinishi, Y.; Lund, T.S.; Vasilyev, O.V.; Moin, P. Fully conservative high order finite difference schemes for incompressible flow. *J. Comput. Phys.* **1998**, *143*, 90–124. [CrossRef]
37. Harlow, F.H.; Welch, J.E. Numerical calculation of time-dependent viscous incompressible flow of fluid with a free surfac. *Phys. Fluids* **1965**, *8*, 2182. [CrossRef]
38. National Institute of Standards and Technology NIST. *Fire Dynamics Simulator Technical Reference Guide, Volume 1: Mathematical Model*; National Institute of Standards and Technology: Gaithersburg, MD, USA, 2018. [CrossRef]
39. Smagorinsky, J. General Circulation Experiments with the Primitive Equations. The Basic Experiment. *Mon. Weather Rev.* **1963**, *91*, 99–164. [CrossRef]
40. Lilly, D.K. The representation of small-scale turbulence in numerical simulation experiments. In Proceedings of the IBM Scientific Computing Symposium on Environmental Sciences, Yorktown Heights, NY, USA, 14–16 November 1966.
41. *European Standards EN15251*; Indoor Environmental Input Parameters for Design and Assessment of Energy Performance of Buildings Addressing Indoor Air Quality, Thermal Environment, Lighting and Acoustics. European Standards s.r.o: Pilsen, Czech Republic, 2007.
42. *European Standards EN 16798-1*; Energy Performance of Buildings—Ventilation for Buildings—Part 1: Indoor Environmental Input Parameters for Design and Assessment of Energy Performance of Buildings Addressing Indoor Air Quality, Thermal Environment, Lighting and Acoustics. European Standards s.r.o: Pilsen, Czech Republic, 2019.
43. Arens, E.; Hoyt, T.; Zhou, X.; Huang, L.; Zhang, H.; Schiavon, S. Modelling the comfort effects of short-wave solar radiation indoors. *Build. Environ.* **2015**, *88*, 3–9. [CrossRef]

44. *ISO-7730*; Ergonomics of the Thermal Environment—Analytical Determination and Interpretation of Thermal Comfort Using Calculation of the PMV and PPD Indices and Local Thermal Comfort Criteria. ISO: Geneva, Switzerland, 2005.

45. Ferrucci, M.; Peron, F. Detailed comfort analysis of the cooling system in the 16th century Villa Aeolia (Costozza, Italy). *IOP Conf. Ser. Mater. Sci. Eng.* **2019**, *609*, 032024. [CrossRef]